Progress In Electromagnetics Research, Vol. 176, 1–10, 2023

Exceptional Ring by Non-Hermitian Sonic Crystals

Bing-Bing Wang[1], Yong Ge[1], Shou-Qi Yuan[1], Ding Jia[1, *], and Hong-Xiang Sun[1, 2, *]

Abstract—Exceptional point (EP) and exceptional ring (ER) are unique features for non-Hermitian systems, which have recently attracted great attentions in acoustics due to their rich physical significances and various potential applications. Despite the rapid development about the study of the EP and ER in one-dimensional acoustic systems, the realization of them in two-dimensional (2D) non-Hermitian structures is still facing a great challenge. To overcome this, we numerically and theoretically realize an ER in 2D reciprocal space based on a square-lattice non-Hermitian sonic crystal (SC). By introducing radiation loss caused by circular holes of each resonator in a Hermitian SC, we realize the conversion between a Dirac cone and the ER. Based on the theoretical analysis with the effective Hamiltonian, we obtain that the formation of the ER is closely related to different radiation losses of dipole and quadrupole modes in the resonators. Additionally, in the non-Hermitian SC, two eigenfunctions can be merged into a single self-orthogonal one on the ER, which does not exist in the Hermitian SC. Finally, by verifying the existence of the EP with topological characteristics in every direction of 2D reciprocal space, we further demonstrate the ER in the proposed non-Hermitian SC. Our work may provide theoretical schemes and concrete methods for designing various types of non-Hermitian acoustic devices.

1. INTRODUCTION

In recent years, non-Hermitian physics has attracted great attention owing to its rich physical significances and various practical applications [1–4]. Exceptional point (EP) is a unique feature for non-Hermitian systems, which has become a hot topic in photonics [5–19], mechanics [20–26], and acoustics [27–39] owing to its great potential in energy transport. In acoustics, based on parity-time symmetric systems [27–32], researchers have realized EP by introducing balanced gain and loss which can be obtained by a pair of electro-acoustic resonators loaded with specifically tailored circuits [30] and by a composite structure composed of a leaky waveguide and two speaker arrays [31]. Additionally, by inserting sound-absorbing sponges in surface holes of coupled cavities, EP can also be obtained in non-Hermitian structures with asymmetric losses [33, 34]. Based on exotic characteristics of EPs [29, 31, 35–37], several advanced acoustic devices have been proposed, such as sound absorber [27], focusing lens [28, 32], invisible acoustic sensor [30], and acoustic mirror [38].

Beyond that, owing to unique and unexpected features, exceptional ring (ER) composed of a continuous closed trajectory of EPs in reciprocal space has initiated an intense research effort in photonics [40–43], cold atoms [44] and acoustics [45]. In photonics, by introducing unequal non-Hermitian perturbations into different modes [40] or sublattices [41–43], researchers have realized ER theoretically [41, 42] and experimentally [40, 43]. In acoustics, based on gain and loss in resonant cavities caused by feedback circuits, a Weyl ER has been realized in a three-dimensional (3D) parameter space

Received 3 September 2022, Accepted 14 October 2022, Scheduled 29 October 2022

* Corresponding author: Ding Jia (jiading@ujs.edu.cn), Hong-Xiang Sun (jsdxshx@ujs.edu.cn).

[1] Research Center of Fluid Machinery Engineering and Technology, School of Physics and Electronic Engineering, Jiangsu University, Zhenjiang 212013, China. [2] State Key Laboratory of Acoustics, Institute of Acoustics, Chinese Academy of Sciences, Beijing 100190, China.

by using a one-dimensional sonic crystal (SC) [45]. To realize an ER in two-dimensional (2D) non-Hermitian SCs by using the same method, it inevitably involves a large number of feedback circuits to achieve sound modulations, which still faces a great challenge owing to the difficulties for controlling these feedback circuits simultaneously.

In this work, we numerically and theoretically realize an ER in 2D reciprocal space based on a non-Hermitian SC. By introducing radiation loss through open circular holes of each resonator in a Hermitian SC, we realize the conversion between a Dirac cone and an ER. Additionally, based on the theoretical analysis with the effective Hamiltonian, we obtain that the formation of the ER is closely related to different radiation losses of dipole and quadrupole modes in the resonators, in which the theoretical predictions and simulated results agree well with each other. Moreover, in non-Hermitian SC, two eigenfunctions can be merged into a single self-orthogonal one on the ER, which cannot be realized by the Hermitian system. Finally, we discuss the topological characteristic of the EP and the existence of the EP in every direction of 2D reciprocal space, which further demonstrate the ER in the designed non-Hermitian SC.

2. RESULTS AND DISCUSSIONS

As schematically shown in Figure 1(a), we propose a type of square-lattice Hermitian SC (with a lattice constant $a = 80\,\mathrm{mm}$) which is composed of periodic resonators (with a diameter of $d = 0.8a$ and a height of $h = 0.88a$) connected by air tubes with a diameter of $d_1 = 0.5242a$. The SC is a closed structure and is filled with air, in which the gain or loss of material is not introduced. Additionally, by introducing open circular holes with the same sizes on top and bottom surfaces of each resonator, we design a type of non-Hermitian SC [Figure 1(b)], in which sound energy can be radiated into outside air from the surface holes. Here, the diameter and height of the holes are set as $d_2 = 0.48a$ and $h_1 = 0.1a$, respectively, and the height of the resonators is adjusted as $h_2 = a$, which is slightly different from the parameter h in Figure 1(a) owing to the change of the eigenfrequencies of the resonator caused by the circular holes. Throughout this work, we use the COMSOL Multiphysics software to numerically simulate acoustic propagation characteristics. All colored surfaces of both SCs in Figure 1 are set as sound hard boundaries. The material parameters of air in the simulation are adopted as follows: the density $\rho_0 = 1.21\,\mathrm{kg/m^3}$ and sound velocity $c_0 = 343\,\mathrm{m/s}$.

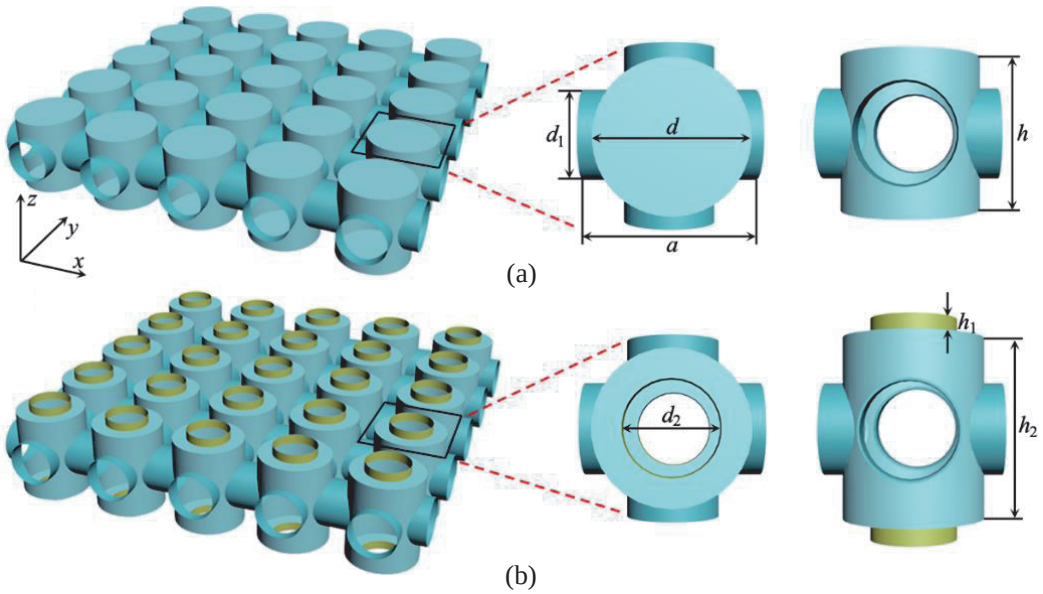

Figure 1. (a) Schematic of a Hermitian square-lattice SC composed of resonators connected with air tubes. (b) Schematic of a non-Hermitian square-lattice SC by introducing circular holes with the same sizes on top and bottom surfaces of each resonator. Insets on the right represent the unit cells of the Hermitian and non-Hermitian SCs.

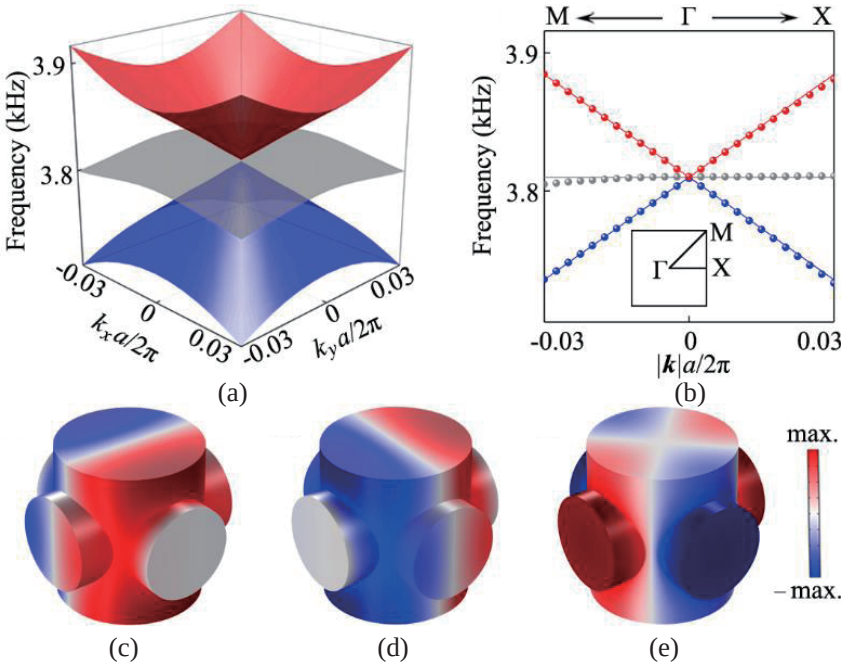

Figure 2. Dispersion relations of the Hermitian SC (a) in 2D reciprocal space and (b) in M-Γ-X direction. Black open square represents the 1st BZ, and colored points and solid lines represent simulated and theoretically calculated results, respectively. Simulated pressure amplitude eigenfunctions at the Γ point for (c) blue, (d) grey and (e) red bands in (b).

Figure 2(a) presents the simulated dispersion relations of the Hermitian SC around the Brillouin zone (BZ) center in the 2D reciprocal space, and the corresponding results in the M-Γ-X direction are displayed in Figure 2(b). We can see that there exists a triply degenerate Dirac point in the BZ center, and the pressure eigenfunctions at the Dirac point are shown in Figures 2(c)–2(e), including two dipole modes and a quadrupole mode. Here, by introducing radiation loss caused by the circle holes of the resonators, the Dirac cone is deformed as the ER. Figures 3(a) and 3(b) present the real and imaginary parts of dispersion relations for the non-Hermitian SC, and the corresponding results along M-Γ-X direction are shown in Figures 3(c) and 3(d). We can see that two bands (marked in red and blue) intersect with each other around the BZ center, which leads to the formation of the ER (green open circle). As shown in Figures 3(a)–3(d), the real and imaginary parts of the dispersion relations are degenerate inside and outside the green open circle, respectively. Additionally, both the real and imaginary parts of the red and blue bands are degenerate on the green open circle, showing typical characteristics of the ER. Here, it is worth noting that the formation of the ER is closely related to different radiation losses of the eigenmodes for the blue and red bands at the Γ point, and has nothing to do with the dispersionless grey band. As shown in Figure 3(d), for the blue band at the Γ point, the imaginary part of the eigenfrequency can reach about 67 Hz, indicating that its corresponding dipole mode [Figure 3(e)] radiates into outer space through the holes. But for the red band, the imaginary part of the eigenfrequency is almost zero at the Γ point, which indicates that its corresponding quadrupole mode [Figure 3(g)] does not radiate due to the mismatched symmetry with the plane wave [40]. The different loss characteristics of the dipole and quadrupole modes play an important role in the formation of the ER.

Next, we theoretically calculate dispersion characteristics of the Hermitian SC by using an effective Hamiltonian. Based on the first-order degenerate perturbation theory [40], the effective Hamiltonian of the Hermitian SC can be written as

$$H = \begin{pmatrix} \omega_0 & v|\mathbf{k}| & 0 \\ v|\mathbf{k}| & \omega_0 & 0 \\ 0 & 0 & \omega_0 \end{pmatrix}, \tag{1}$$

where ω_0, v, and $|\mathbf{k}|$ are the circular frequency at the Dirac point, the group velocity of the linear dispersion, and the amplitude of the in-plane wavevector, respectively. Thus, the eigenvalues of the Hermitian effective Hamiltonian are calculated as

$$\omega = \omega_0, \omega_0 \pm v|\mathbf{k}|. \tag{2}$$

Based on Eq. (2), we can theoretically calculate the dispersion relations [solid lines in Figure 2(b)] of the Hermitian SC, which agree well with the simulated ones.

Additionally, we theoretically present the physical mechanism of the formation of the ER. Here, based on the analysis in Figure 3, we obtain that the dipole modes can be radiated into the outer space through the holes of each resonator, while the quadrupole mode does not radiate [40]. This non-Hermitian perturbation can be described by adding a loss term $i\gamma$ into the Hamiltonian for the dipole

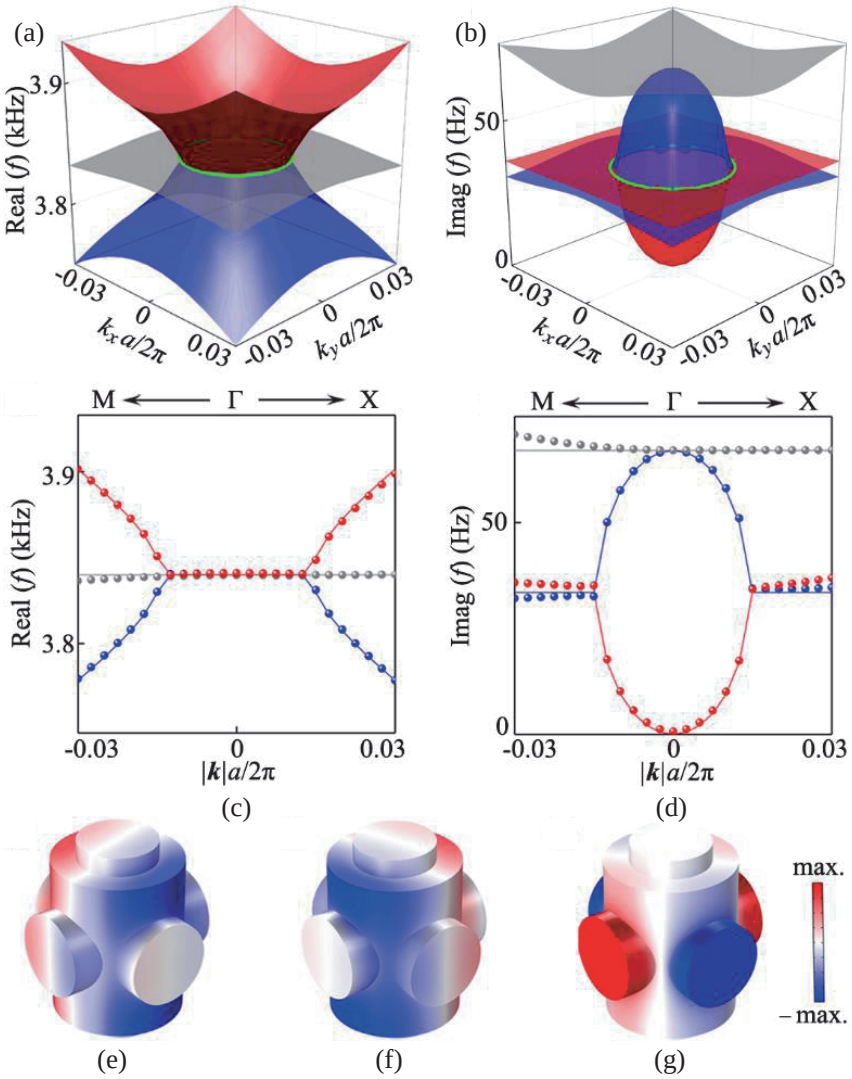

Figure 3. (a) Real and (b) imaginary parts of simulated dispersion relations for the non-Hermitian SC. Green open circles represent the ER. (c) Real and (d) imaginary parts of the dispersion relations in M-Γ-X direction. Colored points and solid lines represent simulated and theoretically calculated results, respectively. Simulated pressure amplitude eigenfunctions at the Γ point for the (e) blue, (f) grey and (g) red bands.

modes. Therefore, the effective Hamiltonian of the non-Hermitian SC is expressed as

$$H = \begin{pmatrix} \omega_0 & v|\mathbf{k}| & 0 \\ v|\mathbf{k}| & \omega_0 + i\gamma & 0 \\ 0 & 0 & \omega_0 + i\gamma \end{pmatrix}. \tag{3}$$

Based on Eq. (3), we can theoretically calculate the eigenvalues of the effective Hamiltonian as

$$\omega = \omega_0 + i\gamma, \omega_0 + i\frac{\gamma}{2} \pm v\sqrt{|\mathbf{k}|^2 - \left(\frac{\gamma}{2v}\right)^2}. \tag{4}$$

Here, it is noted that the dispersionless grey band $\omega = \omega + i\gamma$ in Eq. (4) is decoupled from the other two bands, which is not discussed below. We can see that, on the ring ($|\mathbf{k}| = \gamma/2v$) in 2D reciprocal space, both real and imaginary parts of the eigenfrequencies are degenerate, exhibiting a typical characteristic of the ER. The theoretically calculated dispersion relations of the non-Hermitian SC (solid lines) are shown in Figures 3(c) and 3(d), which agree well with the simulated ones (colored points). Therefore, we theoretically demonstrate that the formation of the ER is closely related to different radiation losses of the dipole and quadrupole modes. Beyond that, it is worth pointing out that when the radiation losses of the dipole and quadrupole modes are the same, the two bands are calculated as $\omega = \omega + i\gamma \pm v|\mathbf{k}|$, forming the Dirac cone instead of the ER.

In addition to the characteristics of eigenfrequencies, we can obtain that the two eigenfunctions in the non-Hermitian SC can be merged into a single one on the ER based on Eq. (3), which does not exist in the Hermitian SC. To present this characteristic, we simulate the pressure amplitude eigenfunctions of both SCs at $|\mathbf{k}| = 0$ and $\gamma/2v$ in Γ-X direction, corresponding to the points A-H in Figure 4. Figure 4(a) presents the simulated dispersion relations of the Hermitian SC around the BZ center in Γ-X direction, in which the corresponding pressure amplitude eigenfunctions at the points A-D are shown in Figures 4(b) and 4(c). As shown in Figure 4(b), a dipole mode (Ψ_1) and a quadrupole mode (Ψ_2) are degenerate at points A and B, which are orthogonal to each other based on the inner product of their pressure distributions. Additionally, by using the basis $\{\Psi_1, \Psi_2\}$, the eigenfunctions at points C and D [Figure 4(c)] are characterized as $\Psi_1 \pm \Psi_2$, respectively. The two eigenfunctions are also orthogonal based on the inner product, which agree well with the theoretical predictions in Eq. (1). Furthermore, for the non-Hermitian SC [shown in Figures 4(d) and 4(e)], a dipole mode (Ψ_1) and a quadrupole mode (Ψ_2) are degenerate and orthogonal at points E and F as well. However, the two eigenfunctions at points G and H [Figure 4(f)] are almost the same and can be characterized as $\Psi_1 - i\Psi_2$. We therefore obtain that both eigenfunctions can be merged into a single self-orthogonal eigenfunction on the ER, which is different from that in the Hermitian SC and is consistent with the theoretical predictions in Eq. (3).

It is worth noting that the EPs on the ER have topological characteristics [3, 44]. To present it, we develop an effective Hamiltonian model, in which the eigenfrequencies of the dipole and quadrupole modes are denoted as ω_1 and ω_2, respectively. In the theoretical model, the parameters v and γ are approximately regarded as constants. Therefore, the corresponding effective Hamiltonian is given as

$$H = \begin{pmatrix} \omega_2 & v|\mathbf{k}| \\ v|\mathbf{k}| & \omega_1 + i\gamma \end{pmatrix}, \tag{5}$$

and the eigenvalues of the effective Hamiltonian are calculated as

$$\omega_\pm = \frac{\omega_1 + \omega_2 + i\gamma}{2} \pm \frac{1}{2}\sqrt{(i\gamma + \omega_1 - \omega_2)^2 + 4v^2|\mathbf{k}|^2}. \tag{6}$$

By substituting $A(|\mathbf{k}|) = \sqrt{[(\omega_1 - \omega_2)^2 + 4v^2|\mathbf{k}|^2 - \gamma^2]^2 + 4\gamma^2(\omega_1 - \omega_2)^2}$, $\sin\theta = 2\gamma(\omega_1 - \omega_2)/A(|\mathbf{k}|)$ and $\cos\theta = [(\omega_1 - \omega_2)^2 + 4v^2|\mathbf{k}|^2 - \gamma^2]/A(|\mathbf{k}|)$ in Eq. (6), we can obtain

$$\omega_\pm = \frac{\omega_1 + \omega_2 + i\gamma}{2} \pm \frac{1}{2}\sqrt{A(|\mathbf{k}|)}e^{i\theta/2}, \tag{7}$$

where $u = \frac{1}{2}\sqrt{A(|\mathbf{k}|)}e^{i\theta/2}$ is a complex square-root function with a branch point at $A(|\mathbf{k}|) = 0$ which is the second-order EP in the effective Hamiltonian. To obtain the relationships between parameters ω_1, ω_2, and d, we simulate the eigenfrequencies of the non-Hermitian SC with different values of d at

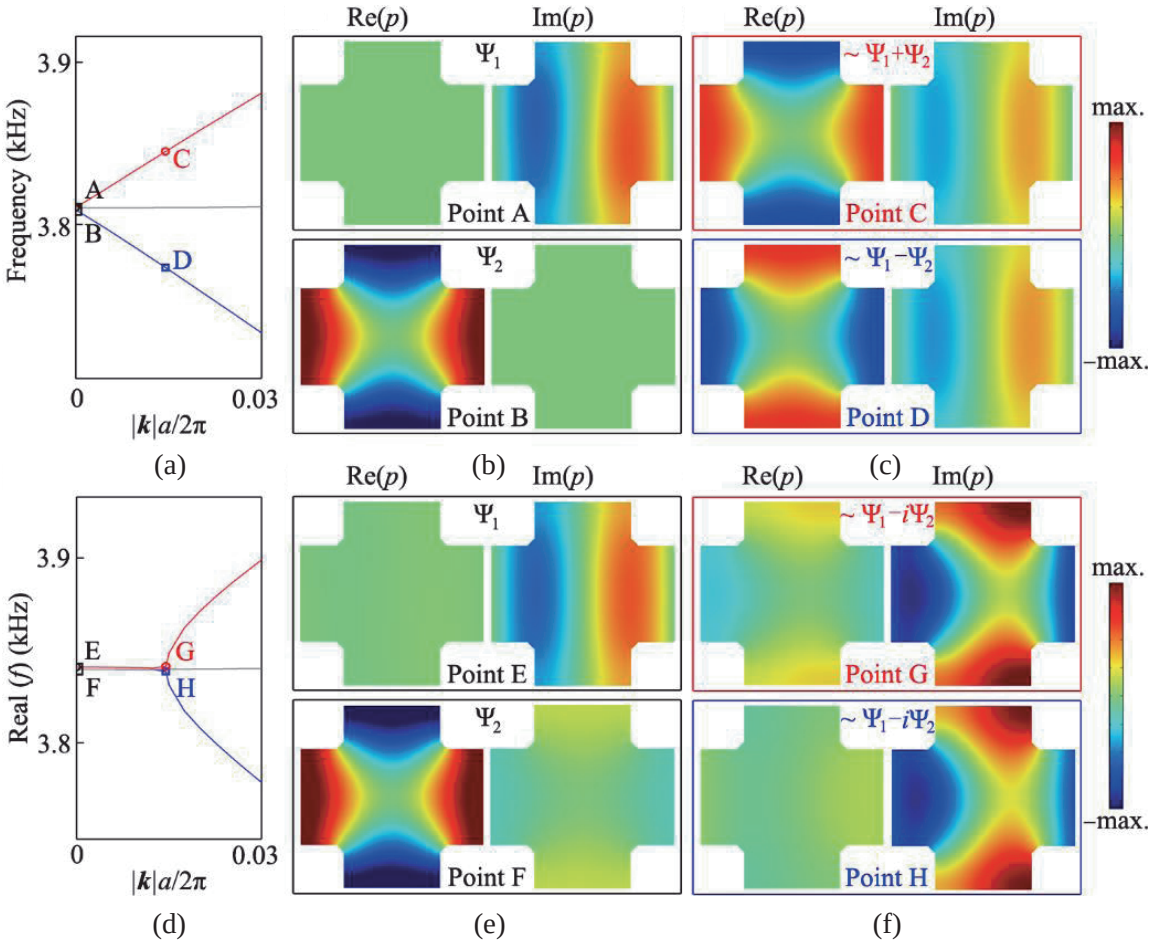

Figure 4. (a) Simulated dispersion relations of the Hermitian SC in Γ-X direction. Pressure amplitude eigenfunctions at the central horizontal cross section in the resonators of Hermitian SC at points (b) A, B and (c) C, D in (a). (d) Simulated dispersion relations of the non-Hermitian SC in Γ-X direction. Pressure amplitude eigenfunctions at the central horizontal cross section in the resonators of the non-Hermitian SC at points (e) E, F and (f) G, H in (d).

the Γ point, and obtain $\omega_1 = [1 - 0.854(d - d_0)/a]\omega_0$ and $\omega_2 = [1 + 0.786(d - d_0)/a]\omega_0$ by using the linear fitting method in which d_0 and ω_0 are the corresponding values at the EPs. Thus, we can rewrite Eq. (7) as

$$\omega_\pm = \frac{[2 - 0.068(d - d_0)/a]\omega_0 + i\gamma}{2} \pm \frac{1}{2}\sqrt{A(|\mathbf{k}|)}e^{i\theta/2}, \tag{8}$$

where $A(|\mathbf{k}|) = \sqrt{[(1.64\frac{d-d_0}{a}\omega_0)^2 + 4v^2|\mathbf{k}|^2 - \gamma^2]^2 + 4\gamma^2(1.64\frac{d-d_0}{a}\omega_0)^2}$, $\sin\theta = -2\gamma(1.64\frac{d-d_0}{a}\omega_0)/A(|\mathbf{k}|)$ and $\cos\theta = [(1.64\frac{d-d_0}{a}\omega_0)^2 + 4v^2|\mathbf{k}|^2 - \gamma^2]/A(|\mathbf{k}|)$.

As shown in Figure 5(a), we select the loop path I (red open rectangle) which encircles a branch point (black point) in the 2D parameter space of $|\mathbf{k}|$ and d. Additionally, we further calculate the values of θ along the loop path I based on Eq. (8) [red open quadrilateral in Figure 5(b)], in which the values of θ change in the whole range of 2π through loop path I. Based on Eq. (8), we can obtain that the two eigenvalues ω_+ and ω_- are exchanged with each other through the loop path I. However, for loop path II [blue open rectangle in Figure 5(a)] without the branch point, the value of θ cannot cover a whole 2π range [blue open quadrilateral in Figure 5(b)] and returns to its initial value at the end of the loop, and therefore the eigenvalues do not exchange with each other based on Eq. (8). Therefore, we theoretically demonstrate the topological characteristic of the EP which is closely related to the properties of the

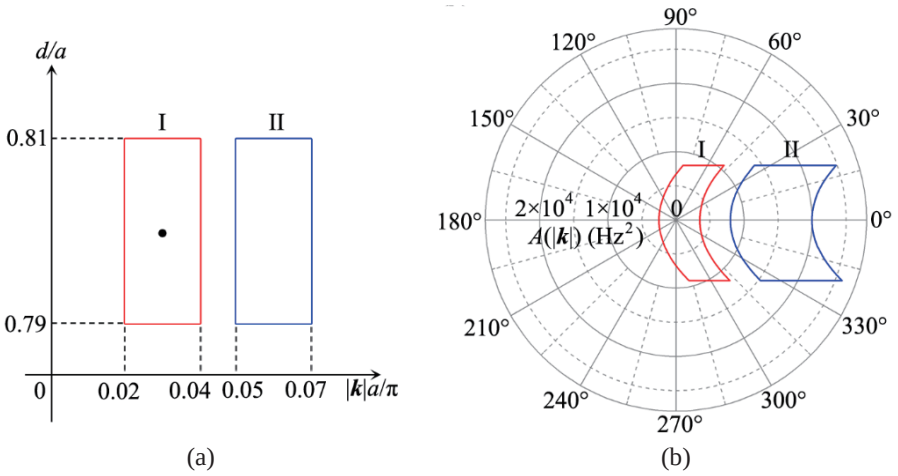

Figure 5. (a) Schematic of two selected loop paths I and II in the 2D parameter space. The black point represents the branch point of the complex square-root function in Eq. (7). (b) The corresponding values of θ along the two loop paths in (a).

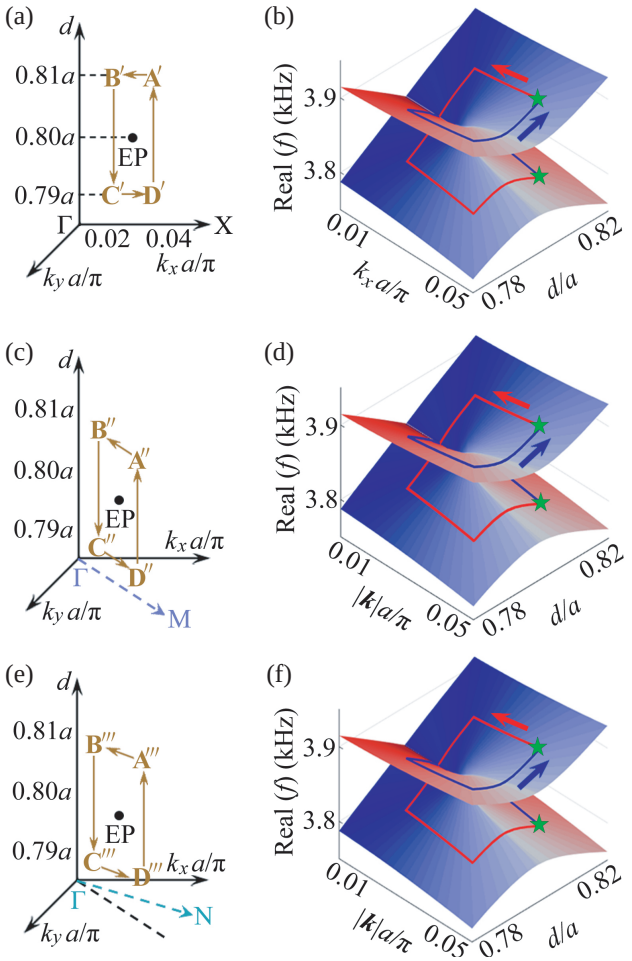

Figure 6. (a) Schematic of a selected loop in Γ-X direction. (b) Distributions of eigenfrequencies (red and blue lines) along the loop path in (a). Green star represents the starting point A of the loop in (a). Similar to (a) and (b), the corresponding results in (c), (d) Γ-M and (e), (f) Γ-N directions.

complex square-root function.

Finally, based on the topological characteristic of the EP, we further demonstrate the existence of the ER in the non-Hermitian SC by verifying the phenomenon that the EP exists in every wavevector direction of the 3D parameter space (composed of the two in-plane wavevectors k_x and k_y and the diameter of the resonator d). Here, we select 3 loops in 3D parameter space arbitrarily and verify the existence of the EP in the corresponding wavevector directions. As shown in Figure 6(a), the loop $A'B'C'D'A'$ is selected in Γ-X direction, and we can obtain that there exists an EP inside the loop based on the result in Figure 3. To verify it, we simulate the associated eigenfrequencies along this loop, which is shown in Figure 6(b). We can see that two eigenfrequencies exchange their positions through the loop path, demonstrating the existence of an EP in Γ-X direction. Additionally, in Γ-M and Γ-N directions [Figures 6(c) and 6(e)], the two eigenfrequencies still exchange the positions with each other through their loop paths [Figures 6(d) and 6(f)], which demonstrates that the EPs also exist in Γ-M and Γ-N directions. The existence of the EP in any other direction of the 2D reciprocal space can also be verified by using the similar method. Therefore, the existence of the ER in the proposed non-Hermitian SC is further demonstrated.

3. CONCLUSIONS

In conclusion, we have realized an ER in a square-lattice non-Hermitian SC which is composed of connected periodic resonators with open circular holes on their top and bottom surfaces. Based on radiation loss caused by circular holes of each resonator in the non-Hermitian SC, we can convert a Dirac cone in a Hermitian SC without circular holes into an ER. It is noted that the radiation loss can be modulated by adjusting the open circular holes, which is more convenient, accurate, and simpler than that caused by using sponges. The formation of the ER is closely related to different radiation losses of dipole and quadrupole modes in the resonators of the non-Hermitian SC, which is theoretically demonstrated by using the effective Hamiltonian. Moreover, we simulate the pressure eigenfunctions in the resonators of both types of SCs and obtain that two eigenfunctions can be merged into a single self-orthogonal one on the ER, which does not exist in the Hermitian SC. Furthermore, we theoretically demonstrate the topological characteristic of the EP and numerically discuss the existence of the EP in 3 selected directions (Γ-X, Γ-M, and Γ-N) of 2D reciprocal space, which can be further used to demonstrate the ER in the non-Hermitian SC. The proposed non-Hermitian SC provides a new route for realizing the ER in 2D acoustic systems, which have great potential in various applications.

ACKNOWLEDGMENT

This work was supported by the National Natural Science Foundation of China (Grant Nos. 12174159 and 12274183), the National Key R&D Program of China (Grant No. 2020YFC1512403), the China Postdoctoral Science Foundation (Grant No. 2020M671351), the Postdoctoral Research Funding Program of Jiangsu Province (Grant No. 2021K567C), and the Postgraduate Research and Practice Innovation Program of Jiangsu Province (Grant No. KYCX22_3603).

REFERENCES

1. Bender, C. M. and S. Boettcher, "Real spectra in non-Hermitian Hamiltonians having PT symmetry," *Phys. Rev. Lett.*, Vol. 80, No. 24, 5243, 1998.
2. El-Ganainy, C. M., K. G. Makris, M. Khajavikhan, Z. H. Musslimani, S. Rotter, and D. N. Christodoulides, "Non-Hermitian physics and PT symmetry," *Nat. Phys.*, Vol. 14, No. 1, 11–19, 2018.
3. Gong, Z. P., Y. Ashida, K. Kawabata, K. Takasan, S. Higashikawa, and M. Ueda, "Topological phases of non-Hermitian systems," *Phys. Rev. X*, Vol. 8, No. 3, 031079, 2018.
4. Bergholtz, E. J., J. C. Budich, and F. K. Kunst, "Exceptional topology of non-Hermitian systems," *Rev. Mod. Phys.*, Vol. 91, No. 1, 015005, 2021.

5. Ramezani, H., T. Kottos, R. El-Ganainy, and D. N. Christodoulides, "Unidirectional nonlinear PT-symmetric optical structures," *Phys. Rev. A*, Vol. 82, No. 4, 043803, 2010.
6. Lin, Z., H. Ramezani, T. Eichelkraut, T. Kottos, H. Cao, and D. N. Christodoulides, "Unidirectional invisibility induced by PT-symmetric periodic structures," *Phys. Rev. Lett.*, Vol. 106, No. 21, 213901, 2011.
7. Regensburger, A., C. Bersch, M.-A. Miri, G. Onishchukov, D. N. Christodoulides, and U. Peschel, "Parity-time synthetic photonic lattices," *Nature*, Vol. 488, No. 8, 167–171, 2012.
8. Liu, Z. P., J. Zhang, Ş. K. Ozdemir, B. Peng, H. Jing, X.-Y. Lu, C.-W. Li, L. Yang, F. Nori, and Y. Liu, "Metrology with PT-symmetric cavities: Enhanced sensitivity near the PT-phase transition," *Phys. Rev. Lett.*, Vol. 117, No. 11, 110802, 2016.
9. Chen, W., Ş. K. Ozdemir, G. Zhao, J. Wiersig, and L. Yang, "Exceptional points enhance sensing in an optical microcavity," *Nature*, Vol. 548, No. 8, 192–196, 2017.
10. Hodaei, H., A. U. Hassan, S. Wittek, H. Garcia-Gracia, R. El-Ganainy, D. N. Christodoulides, and M. Khajavikhan, "Enhanced sensitivity at higher-order exceptional points," *Nature*, Vol. 548, No. 8, 187–191, 2017.
11. Chen, P.-Y., M. Sakhdari, M. Hajizadegan, Q. Cui, M. M.-C. Cheng, R. El-Ganainy, and A. Alù, "Generalized parity-time symmetry condition for enhanced sensor telemetry," *Nat. Electron.*, Vol. 1, No. 5, 297–304, 2018.
12. Chong, Y. D., L. Ge, and A. D. Stone, "PT-symmetry breaking and laser-absorber modes in optical scattering systems," *Phys. Rev. Lett.*, Vol. 106, No. 9, 093902, 2011.
13. Liertzer, M., L. Ge, A. Cerjan, A. D. Stone, H. E. Türeci, and S. Rotter, "Pump-induced exceptional points in lasers," *Phys. Rev. Lett.*, Vol. 108, No. 17, 173901, 2012.
14. Feng, L., Z. J. Wong, R.-M. Ma, Y. Wang, and X. Zhang, "Single-mode laser by parity-time symmetry breaking," *Science*, Vol. 346, No. 6212, 972–975, 2014.
15. Hodaei, H., M. A. Miri, M. Heinrich, D. N. Christodoulides, and M. Khajavikhan, "Parity-time-symmetric microring lasers," *Science*, Vol. 346, No. 6212, 975–978, 2014.
16. Doppler, J., A. A. Mailybaev, J. Böhm, U. Kuhl, A. Girschik, F. Libisch, T. J. Milburn, P. Rabl, N. Moiseyev, and S. Rotter, "Dynamically encircling an exceptional point for asymmetric mode switching," *Nature*, Vol. 537, No. 9, 76–79, 2016.
17. Xu, H., D. Mason, L. Jiang, and J. G. E. Harris, "Topological energy transfer in an optomechanical system with exceptional points," *Nature*, Vol. 537, No. 9, 80–83, 2016.
18. Li, Z. P., G. T. Cao, C. H. Li, S. H. Dong, Y. Deng, X. K. Liu, J. S. Ho, and C. W. Qiu, "Non-Hermitian electromagnetic metasurfaces at exceptional points," *Prog. Electromagn. Res.*, Vol. 171, 1–20, 2021.
19. Yan, Q. H., H. S. Chen, and Y. H. Yang, "Non-Hermitian skin effect and delocalized edge states in photonic crystals with anomalous parity-time symmetry," *Prog. Electromagn. Res.*, Vol. 172, 33–40, 2021.
20. Christensen, J., M. Willatzen, V. R. Velasco, and M.-H. Lu, "Parity-time synthetic phononic media," *Phys. Rev. Lett.*, Vol. 116, No. 20, 207601, 2016.
21. Hou, Z. and B. Assouar, "Tunable elastic parity-time symmetric structure based on the shunted piezoelectric materials," *J. Appl. Phys.*, Vol. 123, No. 8, 085101, 2018.
22. Wu, Q., Y. Chen, and G. Huang, "Asymmetric scattering of flexural waves in a parity-time symmetric metamaterial beam," *J. Acoust. Soc. Am.*, Vol. 146, No. 1, 850, 2019.
23. Domínguez-Rocha, V., R. Thevamaran, F. M. Ellis, and T. Kottos, "Environmentally induced exceptional points in elastodynamics," *Phys. Rev. Applied*, Vol. 13, No. 1, 014060, 2020.
24. Shmuel, G. and N. Moiseyev, "Linking scalar elastodynamics and non-Hermitian quantum mechanics," *Phys. Rev. Applied*, Vol. 13, No. 2, 024074, 2020.
25. Kononchuk, R. and T. Kottos, "Orientation-sensed optomechanical accelerometers based on exceptional points," *Phys. Rev. Research*, Vol. 2, No. 2, 023252, 2020.
26. Rosa, M. I. N., M. Mazzotti, and M. Ruzzene, "Exceptional points and enhanced sensitivity in PT-symmetric continuous elastic media," *J. Mech. Phys. Solids*, Vol. 149, 104325, 2021.

27. Achilleos, V., G. Theocharis, O. Richoux, and V. Pagneux, "Non-Hermitian acoustic metamaterials: Role of exceptional points in sound absorption," *Phys. Rev. B*, Vol. 95, No. 14, 144303, 2017.
28. Yang, H., X. Zhang, Y. Liu, Y. Yao, F. Wu, and D. Zhao, "Novel acoustic flat focusing based on the asymmetric response in parity-time-symmetric phononic crystals," *Sci. Rep.*, Vol. 9, 10048, 2019.
29. Zhu, X. F., H. Ramezani, C. Z. Shi, J. Zhu, and X. Zhang, "PT-symmetric acoustics," *Phys. Rev. X*, Vol. 4, No. 3, 031042, 2014.
30. Fleury, R., D. Sounas, and A. Alù, "An invisible acoustic sensor based on parity-time symmetry," *Nat. Commun.*, Vol. 6, 5905, 2015.
31. Shi, C. Z., M. Dubois, Y. Chen, L. Cheng, H. Ramezani, Y. Wang, and X. Zhang, "Accessing the exceptional points of parity-time symmetric acoustics," *Nat. Commun.*, Vol. 7, 11110, 2016.
32. Liu, T., X. Zhu, F. Chen, S. Liang, and J. Zhu, "Unidirectional wave vector manipulation in two-dimensional space with an all passive acoustic parity-time-symmetric metamaterials crystal," *Phys. Rev. Lett.*, Vol. 120, No. 12, 124502, 2018.
33. Ding, K., G. Ma, M. Xiao, Z. Q. Zhang, and C. T. Chan, "Emergence, coalescence, and topological properties of multiple exceptional points and their experimental realization," *Phys. Rev. X*, Vol. 6, No. 2, 021007, 2016.
34. Ding, K., G. Ma, Z. Q. Zhang, and C. T. Chan, "Experimental demonstration of an anisotropic exceptional point," *Phys. Rev. Lett.*, Vol. 121, No. 8, 085702, 2018.
35. Zhu, W., X. Fang, D. Li, Y. Sun, Y. Li, Y. Jing, and H. Chen, "Simultaneous observation of a topological edge state and exceptional points in an open and non-Hermitian acoustic system," *Phys. Rev. Lett.*, Vol. 121, No. 12, 124501, 2018.
36. Shen, C., J. F. Li, X. Y. Peng, and S. A. Cummer, "Synthetic exceptional points and unidirectional zero reflection in non-Hermitian acoustic systems," *Phys. Rev. Materials*, Vol. 2, No. 12, 125203, 2018.
37. Gu, Z., H. Gao, T. Liu, S. Liang, S. An, Y. Li, and J. Zhu, "Topologically protected exceptional point with local non-Hermitian modulation in an acoustic crystal," *Phys. Rev. Applied*, Vol. 15, No. 1, 014025, 2021.
38. Wang, X., X. S. Fang, D. X. Mao, Y. Jing, and Y. Li, "Extremely asymmetrical acoustic metasurface mirror at the exceptional point," *Phys. Rev. Lett.*, Vol. 123, No. 21, 214302, 2019.
39. Jia, D., Y. Wang, Y. Ge, S. Q. Yuan, and H. X. Sun, "Tunable topological refractions in valley sonic crystals with triple valley hall phase transitions," *Prog. Electromagn. Res.*, Vol. 172, 13–22, 2021.
40. Zhen, B., C. W. Hsu, Y. Igarashi, L. Lu, I. Kaminer, A. Pick, S.-L. Chua, J. D. Joannopoulos, and M. Soljačić, "Spawning rings of exceptional points out of Dirac cones," *Nature*, Vol. 525, No. 9, 354–358, 2015.
41. Wang, H. F., B. Y. Xie, S. K. Gupta, X. Y. Zhu, L. Liu, X. P. Liu, M. H. Lu, and Y. F. Chen, "Exceptional concentric rings in a non-Hermitian bilayer photonic system," *Phys. Rev. B*, Vol. 100, No. 16, 165134, 2019.
42. Kolkowski, R., S. Kovaios, and A. F. Koenderink, "Pseudochirality at exceptional rings of optical metasurfaces," *Phys. Rev. Research*, Vol. 3, No. 2, 023185, 2021.
43. Cerjan, A., S. Huang, M. Wang, K. P. Chen, Y. D. Chong, and M. C. Rechtsman, "Experimental realization of a Weyl exceptional ring," *Nat. Photon.*, Vol. 13, No. 9, 623–628, 2019.
44. Xu, Y., S. T. Wang, and L. M. Duan, "Weyl exceptional rings in a three-dimensional dissipative cold atomic gas," *Phys. Rev. Lett.*, Vol. 118, No. 4, 045701, 2017.
45. Liu, J. J., Z. W. Li, Z. G. Chen, W. Y. Tang, A. Chen, B. Liang, G. C. Ma and J. C. Cheng, "Experimental realization of Weyl exceptional rings in a synthetic three-dimensional non-Hermitian phononic crystal," *Phys. Rev. Lett.*, Vol. 129, No. 8, 084301, 2022.